

Microstructure and mechanical behavior of AZ91 Mg alloy processed by equal channel angular pressing

K. Máthi^{a,b}, J. Gubicza^{c,*}, N.H. Nam^c

^a Department of Metal Physics, Charles University, Ke Karlovu 5, 12116 Praha 2, Czech Republic

^b Department of General Physics, Eötvös University, P.O. Box 32, H-1518 Budapest, Hungary

^c Department of Solid State Physics, Eötvös University, P.O. Box 32, H-1518 Budapest, Hungary

Received 28 September 2004; accepted 20 October 2004

Available online 10 December 2004

Abstract

A fine-grained AZ91 alloy was prepared by equal channel angular pressing (ECAP). The evolution of the microstructure and the deformation behavior were investigated as a function of the number of ECAP passes. At room temperature the tensile strength of the ECA pressed specimens is higher than that of the initial state due to the grain refinement and the increase of the dislocation density during ECAP. Above 200 °C the ductility increases due to the increase of the relative fraction of *c* + *a* dislocations and also owing to the breakage of the rod-like Al₁₂Mg₁₇ precipitates during ECAP processing.

© 2004 Elsevier B.V. All rights reserved.

Keywords: Metals; Dislocations and disclinations; X-ray diffraction

1. Introduction

Magnesium alloys, being among the lightest structural materials, are very attractive in many applications. Their excellent strength to weight ratio predestines Mg-based alloys for applications as structural components in automobile and aircraft industries. The disadvantages of these materials are the poor workability because of their hexagonal structure and the degradation of mechanical properties at elevated temperatures [1].

It is well known that materials with small grain size have excellent mechanical properties. Reduction of the mean grain size is expected to increase the yield strength (and also the ultimate tensile strength) at room temperature and to promote superplastic deformation at higher strain rates and/or lower temperatures than those conventionally used for large grain size materials. Ultrafine grained microstructure in metals can be produced by severe plastic deformation (SPD) techniques. One of the most often used SPD method is equal channel an-

gular pressing (ECAP) which results in bulk, homogeneous submicron or nanocrystalline microstructure without reduction of the cross section of the billet [2]. During the repetitive pressing very high strains are achieved. The microstructure developed after ECAP depends on many factors, e.g. rotation of specimens between consecutive passes, number of passes through the die (the increase of total strain) and temperature of deformation [3,4].

The aim of the present paper is to study the effect of ECAP on the microstructure and the mechanical properties of AZ91 magnesium alloy in the temperature range from room temperature to 300 °C.

2. Experimental procedures

2.1. Sample preparation and experimental techniques

The main alloying elements in the AZ91 magnesium alloy studied here are 9 wt.% Al, 1 wt.% Zn and 0.2 wt.% Mn. The alloy was solution heat-treated for 18 h at 413 °C. The heat-treated samples with dimensions of 10 mm × 10 mm × 60 mm

* Corresponding author. Tel.: +36 1 372 2876; fax: +36 1 372 2868.
E-mail address: gubicza@ludens.elte.hu (J. Gubicza).

were pressed through an ECAP die. The angle between the intersecting channels was 90° . The ECAP was carried out at constant temperature of 270°C . The number of ECAP passes was two, four, and eight. The samples coated with molybdenum disulfide (MoS_2) were pressed at a rate of 5 mm/min using route C (i.e. the samples were rotated around their longitudinal axis by 180° after each pass) [4]. The total strain, ε_n , in the specimen after N passes can be estimated as [4,5]:

$$\varepsilon_n = 1.15N \cot \frac{\phi}{2}, \quad (1)$$

where ϕ is 90° . The values of the total strain were 2.3, 4.6 and 9.2 for two, four, and eight passes, respectively.

Tensile specimens were machined from the initial sample and also from the rods produced by ECAP. These specimens had rectangular cross section of $1\text{ mm} \times 2\text{ mm}$ and gauge length of 9 mm . The tensile tests were carried out by an MTS machine in the temperature range from 20 to 300°C at constant strain rate of $5 \times 10^{-4}\text{ s}^{-1}$.

The phase composition of the samples was studied by X-ray diffraction using a Philips Xpert θ - 2θ powder diffractometer with $\text{Cu K}\alpha$ radiation. The microstructure of the specimens was investigated by X-ray peak profile analysis, optical microscopy (Olympus) and scanning electron microscopy (SEM, Tesla B525). The X-ray diffraction peak profiles were measured by a high-resolution diffractometer (Nonius FR591) with rotating Cu anode and a Ge monochromator ($\text{Cu K}\alpha_1$ radiation, $\lambda = 0.15406\text{ nm}$) [6]. The profiles were recorded by a linear position sensitive gas-flow detector (OED 50 Braun, Múnich). The instrumental broadening was negligible compared to the physical broadening of the profiles therefore instrumental correction was not applied.

2.2. Evaluation of X-ray diffraction data

The measured physical X-ray peak profiles were evaluated by means of the multiple whole profile (MWP) fitting procedure, described in detail in reference [7]. In this method, the Fourier coefficients of the experimental profiles are fitted by the theoretical Fourier transforms calculated on the basis of a model of the microstructure. In this model, the crystallites have spherical shape and log-normal size distribution. The lattice strains are assumed to be caused by dislocations. The procedure has six fitting parameters for hexagonal crystals: (i) the median and the variance, m and σ , of the log-normal size distribution function; (ii) the density and the arrangement parameter of dislocations, ρ and M ; and (iii) the q_1 and q_2 parameters in the contrast factors of dislocations. The volume-weighted mean crystallite size, $\langle x \rangle_{\text{vol}}$, was calculated from m and σ using the formula given in reference [7]. The magnitude of M gives the strength of the dipole character of dislocations: a higher M value corresponds to a weaker dipole character and a weaker screening of the displacement fields of dislocations. The q_1 and q_2 parameters of the contrast factors depend on the character of dislocations and therefore enable the determination of the prevailing dislocation slip systems

in the specimen. The q_1 and q_2 values for the eleven possible slip systems in Mg have been calculated according to Kužel and Klimanek [8] and listed in Table 2 in reference [9]. The 11 dislocation slip systems can be classified into three groups based on their Burgers vectors: $b_1 = 1/3\langle 2\ 1\ 1\ 0 \rangle$ ($\langle a \rangle$ -type), $b_2 = \langle 0\ 0\ 0\ 1 \rangle$ ($\langle c \rangle$ -type) and $b_3 = 1/3\langle 2\ 1\ 1\ 3 \rangle$ ($\langle c + a \rangle$ -type). There are 4, 2 and 5 slip systems in the $\langle a \rangle$, $\langle c \rangle$ and $\langle c + a \rangle$ Burgers vector groups, respectively. A computer program was elaborated to determine the Burgers vector population from the measured values of $q_1^{(m)}$ and $q_2^{(m)}$ [10]. First the program selects some slip systems from one of the three groups. In the second step the calculated \bar{C}_{hk0q_1} and \bar{C}_{hk0q_2} values of the selected slip systems are averaged with equal weights, where \bar{C}_{hk0} is the average contrast factor corresponding to the $hk0$ -type of reflections. This procedure is carried out for each Burgers vector group. The relative fractions of the three groups, h_i ($i = 1, 2, 3$) are calculated by solving the following three equations:

$$q_1^{(m)} = \frac{1}{P} \sum_{i=1}^3 h_i b_i^2 (\bar{C}_{hk0q_1})_i, \quad (2)$$

$$q_2^{(m)} = \frac{1}{P} \sum_{i=1}^3 h_i b_i^2 (\bar{C}_{hk0q_2})_i, \quad (3)$$

and

$$\sum_{i=1}^3 h_i = 1 \quad (4)$$

where $(\bar{C}_{hk0q_1})_i$ and $(\bar{C}_{hk0q_2})_i$ are obtained by averaging for the i th Burgers vector group and P is given as $P = \sum_{i=1}^3 h_i b_i^2 (\bar{C}_{hk0})_i$. If the three h_i weights have positive values the program stores them as one of the possible solutions. After examining all the possible combinations of the slip systems, ranges of the three weights are obtained as the final solution. The detailed description of the procedure is given in reference [9].

3. Results and discussion

3.1. Influence of ECAP processing on the microstructure

The ECAP results in a considerable decrease of the grain size of AZ91 alloy. The process of grain refinement can be seen in the optical micrographs of Fig. 1. Fig. 1a shows the initial microstructure after the solution heat treatment. The decomposition of the grain-structure owing to ECAP begins in the grain boundary area, as it can be seen in Fig. 1b, where the microstructure of the specimen deformed by two ECAP passes is shown. After four passes, further grain refinement can be observed (Fig. 1c). Finally, the sample subjected to eight passes has a homogeneous, fine grained microstructure, as it can be seen in Fig. 1d. Mussi [11] has made transmission electron microscopy (TEM) investigations on these

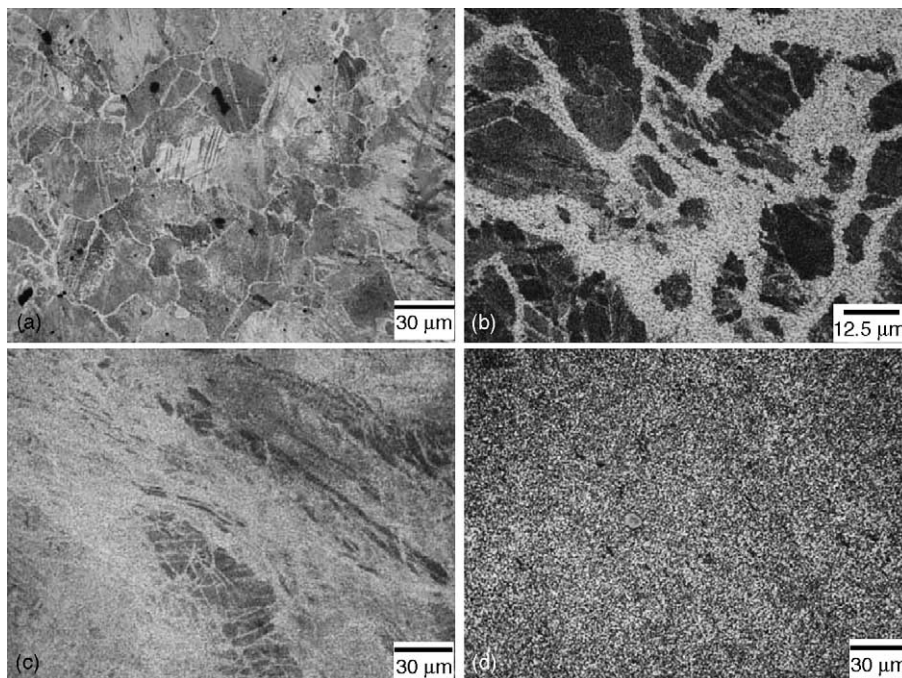


Fig. 1. Optical micrographs of the microstructure for (a) the initial state and the specimens deformed by ECAP for (b) two, (c) four, and (d) eight passes.

specimens. It was found that the initial grain size of $40\ \mu\text{m}$ decreased to $1.2\ \mu\text{m}$ after eight ECAP passes. It should be noted that TEM experiments also revealed that in the latter sample the grains were divided into smaller subgrains with the size of $0.1\ \mu\text{m}$.

The results of the X-ray peak profile analysis confirm the microscopic observation of the refinement of the microstructure due to ECAP. Table 1 shows the volume-weighted mean crystallite size, the dislocation density and the relative fractions of the three Burgers vector types for the initial state and the sample deformed by eight passes. The crystallite size decreases due to ECAP, which is consistent with the microscopic observations. It is worth to note that after eight passes the crystallite size ($97\ \text{nm}$) determined by X-ray peak profile analysis is in good agreement with the subgrain size obtained by TEM ($\sim 100\ \text{nm}$) [11]. Generally, the mean crystallite size determined by X-rays is lower than the grain size observed in the TEM images which has been already reported for SPD materials previously [7]. This can be explained by the fact that the grains in SPD materials are divided into subgrains and/or dislocation cells, which are separated from each other by low angle grain boundaries. The crystallite size in SPD metals obtained by X-ray diffraction is equivalent to the mean size of the domains, which scatter X-rays coherently. Consequently, X-ray diffraction makes a difference between the

dislocation cells (or subgrains), which are separated from each other by small misorientation, typically under $1\text{--}2^\circ$. At the same time it was found previously [7,12] that these dislocation cells could only be observed separately by electron microscopy if highly magnified TEM images were studied very carefully. The usual TEM investigation of SPD metals gives the grain size, which is higher than the dislocation cell or subgrain size obtained by X-ray diffraction peak profile analysis.

The dislocation density increases by a factor of five as a result of eight ECAP passes (see Table 1). It was found, that in the initial state the relative fraction of the $\langle a \rangle$ -type Burgers vectors is the highest. The abundance of this dislocation type beside the $\langle c \rangle$ - and $\langle c+a \rangle$ -type dislocations can be explained by its smallest formation energy. After high temperature ECAP the relative fraction of $\langle c+a \rangle$ -type dislocations increases, which is in agreement with theoretical calculations and former experimental observations [13].

The X-ray diffractogram of the initial specimen after solution heat-treatment is shown in Fig. 2a. Only the reflections of a Mg-based solid solution appear in the diffractogram. The position of the diffraction lines are shifted to higher angles compared with pure Mg due to the reduction of the lattice parameters owing to the alloying Al atoms. At the same time, the high temperature ECA pressing result in the formation of

Table 1

The microstructural parameters of AZ91 alloy for the initial state and after eight ECAP passes

	$\langle x \rangle_{\text{vol}}$ (nm)	ρ ($\times 10^{14}\ \text{m}^{-2}$)	$\langle a \rangle$ -type dislocations (%)	$\langle c \rangle$ -type dislocations (%)	$\langle c+a \rangle$ -type dislocations (%)
Initial state	563	0.4	68–86	0–15	0–14
Eight ECAP	97	2.0	56–58	0–2	38–42

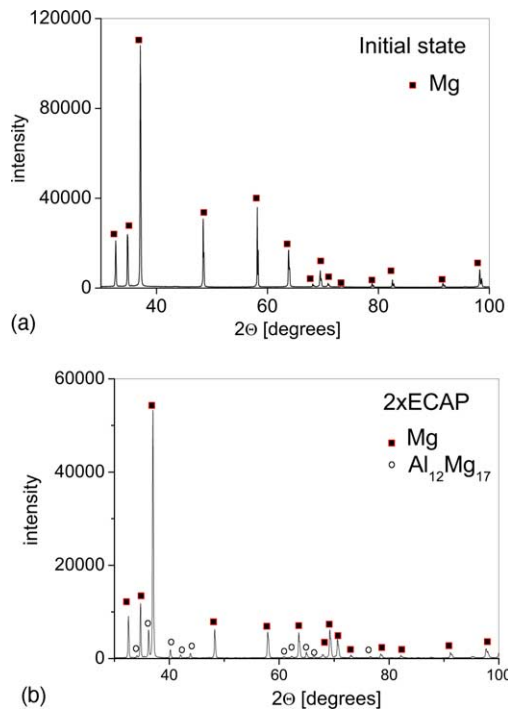


Fig. 2. X-ray diffractograms for (a) the initial state and (b) after two ECAP passes.

Mg₁₇Al₁₂ precipitates from the supersaturated Mg(Al, Zn, Mn) solid solution, as it can be seen for two passes in Fig. 2b. It is worth to note that a common precipitation heat treatment lasts at least for 8 h [1] while the duration of two ECAP passes is approximately 50 min. The precipitation could occur within such a short time because it was facilitated by the severe plastic deformation. Zhang et al. [14] observed similar rapid precipitation during high temperature creep test of Mg–Al alloys. Disk shape continuous and discontinuous precipitates with bcc structure and rod-like shape form during ECAP [15,16] and they play an important role during deformation. Fracture is mostly initiated along them [17] and the fine dispersion of precipitates could improve ductility at high temperature [18]. The shape of precipitates changes during the ECAP processing. Fig. 3a and b shows the SEM micrographs characterizing the microstructure in the weakly and the severely deformed parts of ECAP processed specimens, respectively. The first image is taken from the front part of the specimen after four passes. The second picture is obtained from the internal part of the sample deformed by eight ECAP passes. Comparing the two micrographs it can be established that the discontinuous Mg₁₇Al₁₂ precipitates initially have a long rod-like shape which are broken into smaller parts during ECAP and their dispersion is relatively homogeneous.

3.2. Deformation behaviour of ECAP processed samples

Fig. 4a and b shows the true stress—true strain curves obtained by tension for the initial state and the ECAP pro-

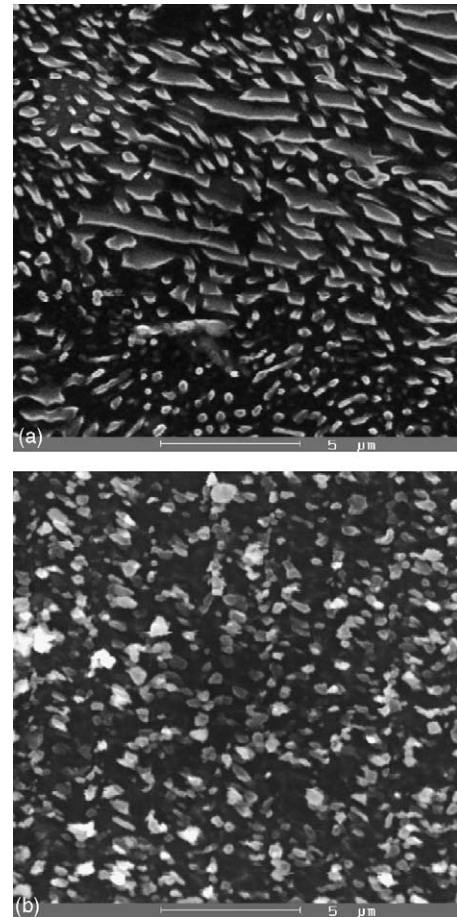


Fig. 3. SEM images on (a) the weakly deformed front part of the sample after four passes and (b) the severely strained internal part of the specimen after eight passes.

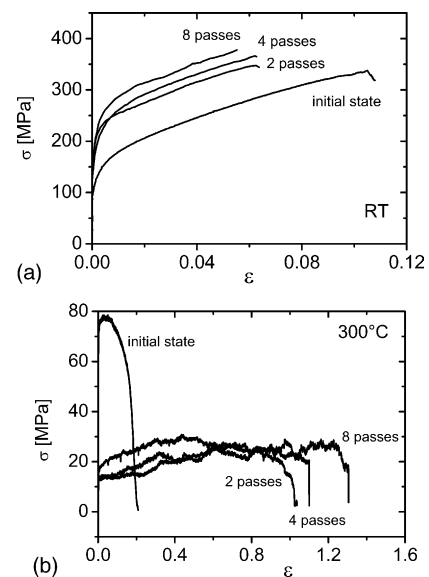


Fig. 4. The true stress—true strain curves for the initial state and for the specimens subjected to ECAP obtained by tension at (a) room temperature and (b) 300 °C.

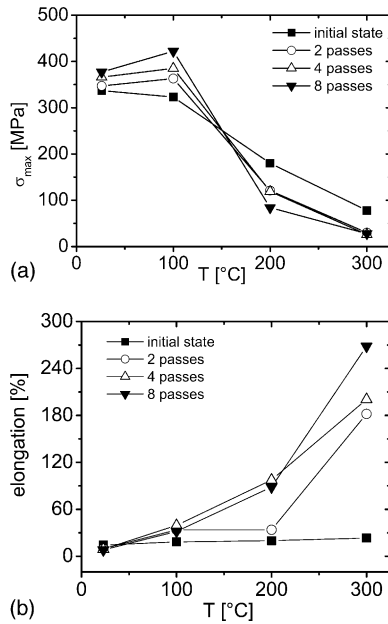


Fig. 5. The tensile strength (a) and the elongation to failure (b) as a function of the deformation temperature.

processed AZ91 specimens at room temperature and 300 °C, respectively. The tensile strength and the elongation to failure obtained from the stress-strain curves are plotted as a function of the deformation temperature in Fig. 5a and b, respectively. The tensile strength was determined as the maximum stress on the true stress–true strain curves and it is denoted by σ_{max} . The elongation to failure is given as the engineering strain in percent. It can be seen, that the ECAP procedure results in the increase of the tensile strength at room temperature as a consequence of the reduction of the grain size as well as the increase of the dislocation density. At the same time at high temperature ($T \geq 200$ °C), where the recovery processes become important, the tensile strength decreases and the ductility increases owing to ECAP. At 300 °C the elongation of the ECAP processed materials achieves the superplastic region (i.e. the engineering strain is higher than 100%). The superplastic behavior is also proved by the value of 0.45 for the strain rate sensitivity parameter ($m = \partial \ln \sigma / \partial \ln \dot{\epsilon}$) obtained by means of strain rate change experiments. From the microstructural analysis and the mechanical testing it can be deduced that at high temperatures the large elongation and the low strength of the ECAP processed specimens compared to the initial state are most probably caused by two phenomena: (i) the breakage of $Al_{12}Mg_{17}$ precipitates into smaller parts which facilitates the dislocation motion (e.g. cross-slip) resulting in the dynamic recovery of the microstructure; (ii) the relatively small grain size which enables the material to deform by the mechanism of grain boundary sliding. Grain boundary sliding plays an important role in superplasticity. The high resolution electron microscopy (HREM) investigation of Mabuchi et al. [19] shows, that the high temperature deformation of AZ91 alloy takes place partly by grain boundary sliding. This phenomenon was also confirmed by

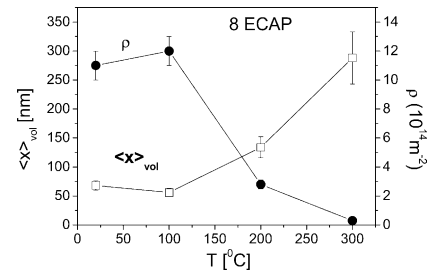


Fig. 6. The volume-weighted mean crystallite size and the dislocation density obtained after tensile test at different temperatures for eight ECAP specimen.

Chuvildev et al. [20], who has found a maximum for both the elongation and the internal friction at 300 °C.

The crystallite size and the characteristic parameters of the dislocation structure were determined for the eight ECAP specimen after tension at different temperatures. The volume-weighted mean crystallite size and the dislocation density as a function of the testing temperature are plotted in Fig. 6. Comparing Figs. 5a and 6, one can deduce that the tensile strength behaves similarly than the dislocation density as a function of the temperature of deformation. Plotting the tensile strength versus the dislocation density, a monotonic relationship can be observed between the two quantities (see Fig. 7). This means that the changes of the tensile strength between room temperature and 300 °C can be attributed mainly to the changes of the dislocation density. The high dislocation densities after room temperature and 100 °C deformation are owing to the dislocation multiplication processes. Dislocation – forest dislocations, dislocation-precipitate and dislocation – grain boundary interactions are responsible for the hardening effects [21,22]. Above 100 °C the dislocation density strongly decreases due to the recovery processes. The dynamic recovery causes strain softening during deformation. Beside the recrystallization, annihilation of dislocations due to the cross-slip of screw dislocations and/or climb of edge dislocations can be taken into account as the mechanisms responsible for softening [23,24].

The activity of non-basal slip systems may also plays an important role in strain softening [25]. Screw dislocations of $\langle c+a \rangle$ -type can move to the next slip planes by double

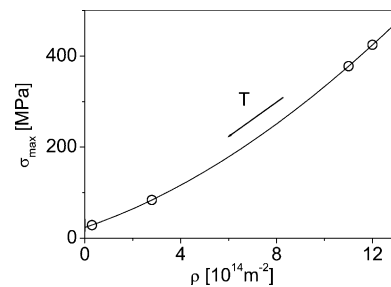


Fig. 7. The monotonic relationship between the dislocation density (ρ) and the tensile strength (σ_{max}) for eight ECAP specimen deformed at different temperatures. The arrow indicates the direction corresponding to the increase of the deformation temperature.

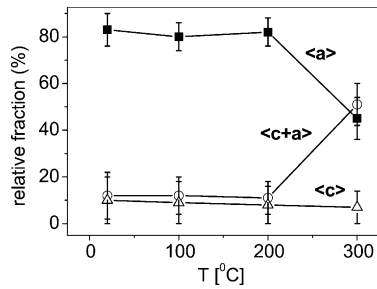


Fig. 8. The relative fractions of the three Burgers vector types as a function of the temperature of tension performed after eight ECAP passes.

cross-slip followed by dislocation annihilation. The activity of the pyramidal system depends strongly on the deformation temperature. At room temperature their critical resolved shear stress is about five times larger than that for basal slip [26], but this value decreases with increasing temperature. Above 200 °C their activation is energetically favorable, as it was shown in our previous work [10]. The Burgers vector population as a function of the deformation temperature is shown for the eight ECAP specimen in Fig. 8. At room temperature, 100 and 200 °C the dominance of $\langle a \rangle$ dislocations can be established. At 300 °C the relative fraction of $\langle c + a \rangle$ dislocations increases at the expense of $\langle a \rangle$ dislocations. It can be established, that at 300 °C the deformation takes place mostly by dislocation glide in pyramidal slip system and by grain boundary sliding.

4. Conclusions

The effect of high temperature ECAP processing on the microstructure and the mechanical properties of AZ91 magnesium alloy was studied by means of optical microscopy, SEM, X-ray line profile analysis and mechanical testing. It is found, that beside the grain refinement, precipitation takes place during ECAP. The reduction of the grain size and the increase of the dislocation density results in the increase of the tensile strength below 100 °C. The shape of $\text{Mg}_{17}\text{Al}_{12}$ precipitates changes owing to ECAP: the rod-like discontinuous precipitates have broken and after eight passes a homogeneous distribution of the precipitates is achieved. This facilitates the recovery of the microstructure during tension above 200 °C, which results in the increase of the ductility. The analysis of the contrast factors shows, that during high temperature deformation the pyramidal $\langle c + a \rangle$ dislocations are also activated and they have a significant contribution to the increase of elongation.

Acknowledgements

This work was supported by the Grant Agency of Academy of Sciences of the Czech Republic under Grant A2041203. The authors are grateful for the financial support of the Hungarian Scientific Research Fund (OTKA) under Contract Numbers F-047057, T-042714 and T-043247.

References

- [1] M.M. Avedesian, H. Baker (Eds.), ASM Specialty Handbook Magnesium and Magnesium Alloys, The Materials Information Society, Materials Park, OH, 1999.
- [2] V.M. Segal, Mater. Sci. Eng. A 197 (1995) 157.
- [3] N.Q. Chinh, Gy. Horváth, Z. Horita, T.G. Langdon, Acta Mater. 52 (2004) 3555.
- [4] K. Nakashima, Z. Horita, M. Nemoto, T.G. Langdon, Mater. Sci. Eng. A 281 (2000) 82.
- [5] V.M. Segal, Mater. Sci. Eng. A 271 (1999) 322.
- [6] T. Ungár, S. Ott, P. Sanders, A. Borbély, J.R. Weertman, Acta Mater. 46 (1998) 3693.
- [7] T. Ungár, J. Gubicza, G. Ribárik, A. Borbély, J. Appl. Cryst. 34 (2001) 298.
- [8] R. Kužel Jr, P. Klimanek, J. Appl. Cryst. 22 (1989) 299.
- [9] I.C. Dragomir, T. Ungár, J. Appl. Cryst. 35 (2002) 556.
- [10] K. Máthis, K. Nyilas, A. Axt, I.C. Dragomir, T. Ungár, P. Lukáč, Acta Mater. 52 (2004) 2889.
- [11] A. Mussi, PhD Thesis, INP Grenoble, 2003.
- [12] Y.T. Zhu, J.Y. Huang, J. Gubicza, T. Ungár, Y.M. Wang, E. Ma, R.Z. Valiev, J. Mater. Res. 18 (2003) 1908.
- [13] S.R. Agnew, O. Duygulu, Mater. Sci. Forum 419–422 (2003) 177.
- [14] P. Zhang, B. Watzinger, Q.P. Kong, W. Blum, Key Eng. Mater. 171–174 (2000) 609.
- [15] S. Maitrejean, M. Veron, Y. Brechet, G.R. Purdy, Scripta Mater. 41 (1999) 1235.
- [16] J.F. Nie, X.L. Xiao, C.P. Luo, B.C. Muddle, Micron 32 (2001) 857.
- [17] G.L. Dunlop, W.P. Sequiera, M.S. Dargusch, G. Song, A. Atrens, T. Kittel, D.H. St John, A.K. Dahle, M. Murray, in: Proceedings of the 55th Meeting of the International Magnesium Association, 1998, p. 68.
- [18] S. Kleiner, O. Beffort, A. Wahlen, P.J. Uggowitzer, J. Light Met. 2 (2002) 277.
- [19] M. Mabuchi, K. Ameyama, H. Iwasaki, K. Higashi, Acta Mater. 47 (1999) 2047.
- [20] V.N. Chuvildeev, T.G. Nieh, M.Yu. Gryaznov, A.N. Sysoev, V.I. Kopylov, Scripta Mater. 50 (2004) 861.
- [21] P. Lukac, Czech J. Phys. B31 (1981) 135.
- [22] Z. Trojanová, P. Lukáč, H. Ferkel, W. Riehemann, Mater. Sci. Eng. A370 (2004) 154.
- [23] Z. Trojanová, Z. Drozd, P. Lukáč, K. Máthis, H. Ferkel, W. Riehemann, Scripta Mater. 42 (2000) 1095.
- [24] K. Máthis, Z. Trojanová, P. Lukáč, Mater. Sci. Eng. A 324 (2002) 141.
- [25] P. Lukáč, K. Máthis, Kovove Mater. 40 (2002) 281.
- [26] M.H. Yoo, Metall. Trans. A 12 (1981) 12.